IEEE Access
Multidisciplinary | Rapid Review | Open Access Journal

Received 3 May 2023, accepted 19 May 2023, date of publication 24 May 2023, date of current version 1 June 2023.

*Digital Object Identifier 10.1109/ACCESS.2023.3279716*

RESEARCH ARTICLE

# Optimal Location and Sizing of Renewable Distributed Generators for Improving Robust Voltage Stability Against Uncontrollable Reactive Compensation

**AKANIT KWANGKAEW[1,2], SIRIYA SKOLTHANARAT[3], CHALIE CHAROENLARPNOPPARUT[2], AND MINEO KANEKO[1], (Member, IEEE)**

[1]School of Information Science, Japan Advanced Institute of Science and Technology, Nomi 923-1292, Japan
[2]School of Information, Computer, and Communication Technology (ICT), Sirindhorn International Institute of Technology (SIIT), Thammasat University, Pathum Thani 12120, Thailand
[3]NECTEC, National Science and Technology Development Agency, Pathum Thani 12120, Thailand

Corresponding author: Akanit Kwangkaew (akanit.kwa@pea.co.th)

This work was supported by the Japan Advanced Institute of Science and Technology (JAIST), Japan.

**ABSTRACT** The penetration level of renewable energy sources is increasing worldwide with incentives and subsidies for declining greenhouse gas emissions. Nevertheless, determining the optimal location and size of renewable distributed generators (RDGs) remains a challenging task, owing to the uncontrollable reactance that dominates power distribution networks in voltage control and its sensitivity to weather conditions. Hence, without considering the reactive compensation of generators, RDG integration incurs undesired total power losses and puts the system at risk for voltage instability and collapse. This research proposes Load Disabling Nodal Analysis for Robust Voltage Stability (LDNA-RVS), a method that determines the optimal location and size of RDGs and aims to improve robust voltage stability by considering reactive compensation while enhancing the loss reduction efficiency (LRE) of the RDG integration. The proposed LDNA-RVS method has been successfully applied to the IEEE 33-bus and IEEE 69-bus test distribution systems, demonstrating its suitability for small-scale systems with a limited number of RDGs. Finally, LDNA-RVS outperforms other methods in six out of eight categories for robust voltage stability and achieves the top rank in all eight categories for LRE. These findings prove the effectiveness of LDNA-RVS in terms of robust voltage stability and LRE against the uncontrollable reactive compensation.

**INDEX TERMS** Reactive compensation, voltage stability, distributed renewable generators, power loss reduction.

## I. INTRODUCTION

Due to the problem of greenhouse gas emissions and the insufficiency of conventional power sources to meet growing energy demand, renewable distributed generators (RDGs) have been increasingly promoted worldwide [1], [2], [3] as an environment-friendly option. However, due to their intermittent nature, the amount of generated power from RDGs (such as photovoltaic (PV) and wind turbine (WT)) is uncontrollable compared to conventional dispatchable sources like oil, natural gas, and coal. As a result, inappropriate sizing and placement of RDGs can lead to increased power losses and degraded voltage stability [4], [5], [6], [7], [8]. In particular, the uncontrollable reactive compensation of these energy sources can lead to voltage stability degradation [8].

The associate editor coordinating the review of this manuscript and approving it for publication was Laura Celentano.

The optimal location and size of RDGs have been the subject of numerous studies. Researchers have focused on developing methodologies that minimize total power losses while determining optimal locations and sizes [9], [10], [11], [12], [13], [14], [15], [16], [17], [18], [19], [20], [21], [22] and improve voltage profiles [10], [13], [15], [17], [21]. In [9], the authors proposed an analytical expression to estimate the optimal size of the distributed generator (DG) and presented a methodology to determine their locations. The authors of [10] determined locations of DGs based on the incremental voltage sensitivity and developed Differential evolution (DE) for obtaining their sizes with considering the minimum losses. The proposed techniques of [10] named Bones particle swarm optimization (BBPSO) and Multi-membered non-recombinative evolution strategy (MMNRES) performed the best result in terms of minimum losses and voltage profile improvement. Genetic algorithm (GA) was used utilized by the authors of [12] and [23] to determine the locations of DGs with considering the losses minimization as the DG installation objective, while the authors of [23] involved energy saving in terms of cost. GA was developed into the augmented Lagrangian genetic algorithm (ALGA) by the authors of [24] for determining the locations of RDGs with minimizing both the losses and investment cost. The authors of [11] formulated the sensitivity factor and employed it to determine the optimum location and size of DGs with minimizing losses using an analytical method and the classical grid search algorithm. The authors of [25] utilized the particle swarm optimization (PSO) technique to solve the optimal placement of DGs while considering the loss minimization. Later on, PSO was developed into the Multileader Particle Swarm Optimization (MLPSO) by the authors of [26], which provided better results. The authors of [14] proposed a Modified Teaching-Learning Based Optimization (MTLBO) to determine the optimal location and size of DGs simultaneously in distribution systems. The authors of [15] determined the optimal placement and size of DGs by minimizing the multi-objective performance index, including active power loss, reactive power loss, voltage profile, and reserve capacity indices and using the supervised Big Bang-Big Crunch (BB-BC) method. The author of [27] managed a swarm optimization technique, namely a Backtracking Search Optimization Algorithm (BSOA), to determine locations and sizes of DGs by adapting the weighting factor in the objective function to reduce losses and enhance the voltage profile. The authors of [16] involved the Ant Lion Optimization Algorithm (ALOA) to determine the optimal placement of RDGs, resulting in the minimum losses. The above methodologies have succeeded in loss minimization and voltage profile improvement. Nevertheless, these studies often neglect voltage stability robustness and reactive compensation, which may lead to increased power loss in case of uncontrollable reactive compensation.

In [28], it is pointed out that the uncontrollable reactive compensation of renewable energy sources can have a significant impact on voltage stability, security against voltage collapse, and the efficiency of reducing power losses in generators. This is because reactive power plays a dominant role in voltage control in power distribution networks. From this perspective, the previous research studies are inadequate as they rarely take reactive compensation into account.

Recently, the authors of [8] reported on the crucial impact of uncontrollable reactive compensation from renewable distributed generators (RDGs) on the voltage stability and security of power systems, and they proposed a methodology that considers the uncontrollable reactive compensation in order to minimize power loss and improve voltage stability. However, they still did not consider the robustness of voltage stability, which could result in adverse consequences, such as increased power losses, decreased efficiency, and a weakened ability to mitigate voltage collapse.

### A. MOTIVATION

To determine appropriate locations and sizes of RDGs is a crucial task for managing a power system. As it is summarized above, there is room for improvement of the location algorithm. The major concerns we focus on include the following.

- Uncontrollable RDGs have the potential to exacerbate power losses due to uncontrollable reactive compensation.
- Employing total power losses as the exclusive objective function might not guarantee effective loss reduction.
- Consequently, a methodology for ascertaining the optimal placement of RDGs should consider voltage stability robustness in the face of uncontrollable reactive compensation.

These insights inspire the development of a more comprehensive and sophisticated approach that addresses both power loss reduction and voltage stability enhancement in determining the optimal location and size of RDGs.

In this study, we introduce a novel index called the Normalized Voltage Stability index ($\Lambda$) and a method named Load-Disabling Nodal Analysis (LDNA) for identifying the optimal location and size of RDGs. Our objective is to enhance voltage stability robustness in the face of uncontrollable reactive compensation while also taking into account the efficiency of power loss reduction efficiency (LRE). Through our discussions and experiments, we show that $\Lambda$ is important for accomplishing two primary objectives of RDG allocation: the improvement of voltage stability and the maximization of LRE.

### B. MAIN CONTRIBUTIONS

The primary contributions of this research include:

- The proposed Load-Disabling Nodal Analysis for Robust Voltage Stability (LDNA-RVS) method addresses the challenge of uncontrollable and weather-

dependent variations in the dominant reactance in power distribution networks, improving robust voltage stability by considering reactive compensation and enhancing the loss reduction efficiency (LRE) of RDG integration.
- The consideration of the challenge posed by uncontrollable and weather-dependent changes in the dominant reactance in power distribution networks, which exposes the system to risks of voltage instability, collapse, and undesirable total power losses.
- The application of the proposed LDNA-RVS method to IEEE 33-bus and IEEE 69-bus test distribution systems, including a comparative analysis with other techniques to demonstrate its effectiveness in terms of robust voltage stability and LRE against uncontrollable reactive compensation.
- The demonstration of the relationship between voltage stability, power loss reduction, and the voltage product function through various case studies.
- The LDNA-RVS method's contribution to enhancing voltage stability and power loss reduction, as well as the proposal of a system voltage stability index.
- The validation of the proposed voltage stability index ($\Lambda$) for identifying optimal RDG installation locations that support both voltage stability improvement and power loss reduction efficiency.

### C. ADVANTAGES
- LDNA-RVS determines the optimal size and location of RDGs by incorporating reactive compensation to enhance robust voltage stability.
- The method also improves the loss reduction efficiency (LRE) of RDG integration, presenting a comprehensive solution for enhancing the incorporation of RDGs into power distribution networks.
- The proposed approach takes into account the non-linear characteristics of reactive compensation, enabling the achievement of minimum power loss.
- This research provides a solution for addressing the challenges associated with RDG integration and attaining sustainable and reliable power generation from renewable sources.

### D. ORGANIZATION AND HIGHLIGHTS
The rest of paper is organized as follows: Section II introduces the preliminary and background, i.e., system model, voltage stability index, power loss, and power loss reduction efficiency. Section III describes the voltage product function, related mathematical key functions, and their contributions. Next, Section IV introduces the proposed method for determining the optimal locations and sizes of RDGs. Section V explains the simulations and results of determining the optimal placement on IEEE 33- and IEEE 69-bus test distribution systems. Finally, Section VI presents the conclusions of the paper and future research directions.

The highlights of this paper include
- Introduction of the voltage-product function and its relations with L-index and power loss reduction.
- Introduction of LDNA as a general framework for finding suitable locations of RDGs.
- Various simulation results which intensively show the performance shifts depending on the reactive power compensation ratio (RCR), and indicate the superiority of the proposed method to the previous approaches under the RCR-induced variability of performances.

## II. PRELIMINARY BACKGROUND
In this section, we provide preliminary background information on the power distribution network and discuss the voltage stability index and loss reduction efficiency as key metrics for evaluating the performance of our proposed method.

### A. SYSTEM MODEL
Information on the power requirement, a single line diagram, and line impedance is provided considering the steady-state situation. The following variables are reserved for representing a given system.

| | |
|---|---|
| $N$ | the number of buses, |
| $\mathcal{N} = \{1, 2, \ldots, N\}$ | the set of bus indices, |
| $N_{RDG}$ | the number of RDGs, |
| $\overline{Y}_{mn}$ | the $m$th row $n$th column complex element of the admittance matrix $Y_{bus}$, |
| $P_k$ | total active power injection at the $k$th bus, |
| $Q_k$ | total reactive power injection at the $k$th bus, |
| $P_k^{RE}$ | generated active power injections of RDG at the $k$th bus, |
| $Q_k^{RE}$ | generated reactive power injections of RDG at the $k$th bus, |
| $\overline{V}_k$ | the complex voltage at the $k$th bus, |
| $\overline{I}_k$ | the complex current injection at the $k$th bus, |
| $V_k$ | the magnitude of the complex voltage $\overline{V}_k$ |
| $\delta_k$ | the angle of the complex voltage $\overline{V}_k$. |

The following assumptions are made for the discussions in this paper.
- The number of generators to be installed is given.
- For any RDG, the reactive compensation required for maintaining the voltage level at an acceptable rate is assumed to be consumed depending on its generated active power multiplied by the reactive power compensation ratio (RCR). Thus, the effect of uncontrollable reactive compensation of an RDG associated with its generated power is evaluated using RCR.
- The power system is assumed to be a three-phase system with balanced voltages.

- Basically, the voltage stability degradation appears on the negative value of RCR or the lagging of the power factor. Thus, for observing the robust voltage stability (RVS) and the safety margin of voltage collapse, the uncontrollable reactive compensation on the negative value of RCR is focused on.
- Energy Star, operated jointly by the Environmental Protection Agency (EPA) and the US Department of Energy (DOE), policies for computing equipment to have a power factor of greater than 0.9 at the rated output in the application's power supply. Accordingly, this paper considers that the power factor ranges from 0.9 lagging to 0.9 leading.

### B. VOLTAGE STABILITY INDEX

For delineating quantitative measurement of a weak bus and forecasting voltage collapse, the L-index proposed by [29] is used as one of the measurements to evaluate a system. In order to achieve robust voltage stability (RVS), the variation of voltage levels needs to be safe from voltage collapse. In this paper, the voltage stability and its robustness against the uncontrollable reactive compensation of RDGs are examined by using the L-index. At the $k$th bus, the L-index is defined as follows [29].

$$L_k = \left| 1 - \frac{\sum_{n\in\alpha_G} \overline{F}_{kn}\overline{V}_n}{\overline{V}_k} \right| \tag{1}$$

where $\alpha_G$ is the set of generator buses. $\overline{F}_{kn}$ is the $k$th row, $n$th column element of the hybrid matrix, which is generated from the admittance matrix $\boldsymbol{Y}_{bus}$ and can be used as a multiplicative factor of $V_n$ to express $V_k$.

In order to describe the stability of the whole system, a global indicator L-index is expressed as follows.

$$L = \max_{k\in\mathcal{N}} L_k \tag{2}$$

Basically, the value of the L-index should be less than 1 for a stable operation. When the voltage collapse happens, the value of the L-index will be equal to 1. The smaller from 1 the value of the L-index is, the more stable the system is. Since the voltage degradation appears on the negative value of RCR or lagging power factor, the worst case of voltage stability is focused. That is, RVS is measured using L-index with 0.9 lagging of the power factor or RCR=−0.48 using the L-index.

### C. LOSS REDUCTION EFFICIENCY

The ability to reduce the active power losses is one of the key factors in choosing the optimal placement of RDGs [8]. In order to reveal the power loss effect regarding power generated from RDGs, first, the system power losses ($P_{loss}$) which is introduced by [30] is calculated with additional power generated from RDGs and the reactive compensation rate (RCR). Now let $\mathcal{RE}$ be the set of indices of buses where RDGs are installed, and let $\mathcal{P}^{\mathcal{RE}}$ be the vector of generated active power of RDGs, i.e.,

$$\mathcal{P}^{\mathcal{RE}} = \left(P^{RE}_{G_1}, P^{RE}_{G_2}, \cdots, P^{RE}_{G_{N_{RDG}}}\right) \in \mathbb{R}^{N_{RDG}}$$

where

$$\mathcal{RE} = \left\{G_1, G_2, \cdots, G_{N_{RDG}}\right\}$$

Let $P'_i = P_i + P^{RE}_i$ for $i \in \mathcal{RE}$, $P'_i = P_i$ otherwise, and $Q'_i = Q_i + Q^{RE}_i$ for $i \in \mathcal{RE}$, $Q'_i = Q_i$ otherwise. Equation (3) shows the power loss computation considering initially installed sources/loads and $P^{RE}_{G_i}$ and $Q^{RE}_{G_i} = RCR \times P^{RE}_{G_i}$ of RDGs to be installed.

$$\begin{aligned} P^{\mathcal{RE}}_{loss}(\mathcal{P}^{\mathcal{RE}}, \mathrm{RCR}) = \sum_{m=1}^{N}\sum_{n=1}^{N}(a_{mn}(P'_mP'_n + Q'_mQ'_n) \\ + b_{mn}\left(Q'_mP'_n - P'_mQ'_n\right)) \end{aligned} \tag{3}$$

with

$$a_{mn} = \frac{r_{mn}}{V_mV_n}\cos(\delta_m - \delta_n),$$
$$b_{mn} = \frac{r_{mn}}{V_mV_n}\sin(\delta_m - \delta_n)$$

where $r_{mn}$ is the element in the $m$th row, $n$th column element of $Re[\boldsymbol{Y}^{-1}_{bus}]$.

Then, loss reduction efficiency (LRE), which is used as the ability of the RDG(s) to reduce the active power losses of the system, can be expressed as follows.

$$\mathrm{LRE} = \frac{P^{\mathcal{RE}}_{loss}(\mathcal{P}^{\mathcal{RE}}, \mathrm{RCR})}{\sum_{i\in\mathcal{RE}} P^{RE}_i} \tag{4}$$

## III. THE CONTRIBUTIONS OF THE VOLTAGE PRODUCTION FUNCTION

In this section, we will recall the voltage product function [8]. Several case studies show how it relates to voltage stability and power loss reduction.

### A. MATHEMATICAL KEY FUNCTIONS

For any $k$th bus, the conjugate complex power $\overline{S}^*$ is given as

$$\begin{aligned} \overline{S}^*_k &= \overline{V}^*_k\overline{I}_k \\ &= \overline{V}^*_k\sum_{n=1}^{N}\overline{Y}_{kn}\overline{V}_n \end{aligned}$$

which can be converted to

$$\frac{\overline{S}^*_k}{\overline{Y}_{kk}} = \left(\sum_{n=1,n\neq k}^{N}\frac{\overline{Y}_{kn}\overline{V}_n}{\overline{Y}_{kk}}\right)\cdot\overline{V}^*_k + V^2_k \tag{5}$$

The voltage product (v-p) function ($\overline{\psi}_k$) at the $k$th bus is defined as

$$\overline{\psi}_k \triangleq \frac{\sum_{n=1,n\neq k}^{N}\overline{Y}_{kn}\overline{V}_n}{\overline{Y}_{kk}} \tag{6}$$

Next, we can rewrite equation (5) by substituting $\overline{\psi}_k$, as shown below.

$$\frac{\overline{S}_k^*}{\overline{Y}_{kk}} = \overline{\psi}_k \overline{V}_k^* + V_k^2 \tag{7}$$

$$= \psi_k V_k \cos(\zeta_k - \delta_k) + j\psi_k V_k \sin(\zeta_k - \delta_k) + V_k^2 \tag{8}$$

where $\psi_k$ and $\zeta_k$ are the v-p magnitude and the v-p angle at the $k$th bus, respectively.

Separating (8) into real and imaginary parts, we define

$$\alpha_k(V_k, \Delta_k, \psi_k) \triangleq V_k^2 + \psi_k V_k \cos(\Delta_k) \tag{9}$$

$$\beta_k(V_k, \Delta_k, \psi_k) \triangleq \psi_k V_k \sin(\Delta_k) \tag{10}$$

where $\Delta_k = \zeta_k - \delta_k$. For simplification, $\alpha_k$ and $\beta_k$ are used for $\alpha_k(V_k, \Delta_k, \psi_k)$ and $\beta_k(V_k, \Delta_k, \psi_k)$, respectively, if the arguments are unambiguous from the context. For calculating the magnitude of the voltage at the $k$th bus using $\alpha_k$, $\beta_k$ and $\psi_k$, we substitute (9) and (10) into (8) to obtain the bus voltage equation as

$$V_k^4 - V_k^2 \left(\psi_k^2 + 2\alpha_k\right) + \alpha_k^2 + \beta_k^2 = 0 \tag{11}$$

With the aid of a complex transformation, (7) can be expressed in a different form.

$$\frac{\overline{S}_k^*}{\overline{Y}_{kk} V_k^2} \& = \frac{\overline{\psi}_k}{\overline{V}_k} + 1 \tag{12}$$

### B. VOLTAGE STABILITY IMPROVEMENT

Voltage stability is defined as the ability to maintain the voltage level of each bus in an acceptable range during regular operation and after any contingency events [31]. However, the nonlinear relationship between the power injection of RDGs and the voltage stability expressed in the formulation of the L-index is challenging to apply to the RDG location and sizing problem. The voltage stability depends not only on voltage levels and power injection of individual node but also on other adjacent buses and system variables. In this paper, we will find that the voltage product function (Equation (6)) plays an important role in the voltage stability issue. The following demonstrates how the function associates with voltage stability improvement using the 3-bus system shown in Fig.1.

Depending on a different choice of reference bus of the 3-bus system, we can have three different network models as shown in Fig.2, where case I, case II and case III are obtained by choosing bus c, bus b and bus a, respectively, as the reference node.

Then, the hybrid parameters of the three cases are obtained as following equations.

**Case (I)**

$$\overline{v}_{ac} = h_{11}^{(\mathrm{I})} \cdot \overline{i}_a^{(\mathrm{I})} + h_{12}^{(\mathrm{I})} \cdot \overline{v}_{bc} \tag{13}$$

$$\overline{i}_b^{(\mathrm{I})} = h_{21}^{(\mathrm{I})} \cdot \overline{i}_a^{(\mathrm{I})} + h_{22}^{(\mathrm{I})} \cdot \overline{v}_{bc} \tag{14}$$

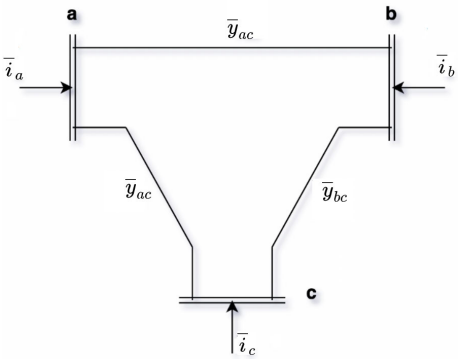


**FIGURE 1.** Single line diagram of the 3-bus system.

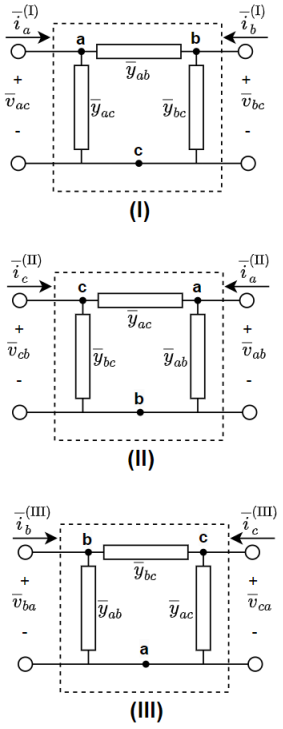


**FIGURE 2.** Three different cases regarding referent buses.

Then, $h_{11}^{(\mathrm{I})}$, $h_{12}^{(\mathrm{I})}$, $h_{21}^{(\mathrm{I})}$ and $h_{22}^{(\mathrm{I})}$ can be computed,

$$h_{11}^{(\mathrm{I})} = \left.\frac{\overline{v}_{ac}}{\overline{i}_a^{(\mathrm{I})}}\right|_{v_{bc}=0} = \frac{\overline{v}_{ac}}{v_{ac} \cdot \overline{y}_{ac} + \overline{v}_{ac} \cdot \overline{y}_{ab}} = \frac{1}{\overline{y}_{ac} + \overline{y}_{ab}}$$

$$h_{12}^{(\mathrm{I})} = \left.\frac{\overline{v}_{ac}}{\overline{v}_{bc}}\right|_{i_a^{(\mathrm{I})}=0} = \frac{\overline{y}_{ab}}{\overline{y}_{ab} + \overline{y}_{ac}}$$

$$h_{21}^{(\mathrm{I})} = \left.\frac{\overline{i}_b^{(\mathrm{I})}}{\overline{i}_a^{(\mathrm{I})}}\right|_{v_{bc}^{(\mathrm{I})}=0} = -\frac{\overline{y}_{ab}}{\overline{y}_{ac} + \overline{y}_{ab}}$$

$$h_{22}^{(\mathrm{I})} = \left.\frac{\bar{i}_b^{(\mathrm{I})}}{\bar{v}_{bc}}\right|_{\bar{i}_a^{(\mathrm{I})}=0} = \bar{y}_{bc} + \left(\frac{\bar{y}_{ab}\cdot\bar{y}_{bc}}{\bar{y}_{ab}+\bar{y}_{bc}}\right)$$

Then,the matrix of hybrid parameters of the Case (I) can be obtained,

$$\begin{bmatrix} h_{11}^{(\mathrm{I})} & h_{12}^{(\mathrm{I})} \\ h_{21}^{(\mathrm{I})} & h_{22}^{(\mathrm{I})} \end{bmatrix} = \begin{bmatrix} \frac{1}{\bar{y}_{ab}+\bar{y}_{ac}} & \frac{\bar{y}_{ab}}{\bar{y}_{ab}+\bar{y}_{ac}} \\ -\frac{\bar{y}_{ab}}{\bar{y}_{ab}+\bar{y}_{ac}} & \bar{y}_{bc} + \left(\frac{\bar{y}_{ab}\cdot\bar{y}_{ac}}{\bar{y}_{ab}+\bar{y}_{ac}}\right) \end{bmatrix}$$

**Case (II)**

$$\bar{v}_{cb} = h_{11}^{(\mathrm{II})}\cdot\bar{i}_c^{(\mathrm{II})} + h_{12}^{(\mathrm{II})}\cdot\bar{v}_{ab} \tag{15}$$

$$\bar{i}_a^{(\mathrm{II})} = h_{21}^{(\mathrm{II})}\cdot\bar{i}_c^{(\mathrm{II})} + h_{22}^{(\mathrm{II})}\cdot\bar{v}_{ab} \tag{16}$$

Then, the matrix of hybrid parameters of the Case (II) can be obtained,

$$\begin{bmatrix} h_{11}^{(\mathrm{II})} & h_{12}^{(\mathrm{II})} \\ h_{21}^{(\mathrm{II})} & h_{22}^{(\mathrm{II})} \end{bmatrix} = \begin{bmatrix} \frac{1}{\bar{y}_{ac}+\bar{y}_{bc}} & \frac{\bar{y}_{ac}}{\bar{y}_{ac}+\bar{y}_{bc}} \\ -\frac{\bar{y}_{ac}}{\bar{y}_{ac}+\bar{y}_{bc}} & \bar{y}_{ab} + \left(\frac{\bar{y}_{ac}\cdot\bar{y}_{bc}}{\bar{y}_{ac}+\bar{y}_{bc}}\right) \end{bmatrix}$$

**Case (III)**

$$\bar{v}_{ba} = h_{11}^{(\mathrm{III})}\cdot\bar{i}_b^{(\mathrm{III})} + h_{12}^{(\mathrm{III})}\cdot\bar{v}_{ca} \tag{17}$$

$$\bar{i}_c^{(\mathrm{III})} = h_{21}^{(\mathrm{III})}\cdot\bar{i}_b^{(\mathrm{III})} + h_{22}^{(\mathrm{III})}\cdot\bar{v}_{ca} \tag{18}$$

Then, the matrix of hybrid parameters of the Case (III) can be obtained,

$$\begin{bmatrix} h_{11}^{(\mathrm{III})} & h_{12}^{(\mathrm{III})} \\ h_{21}^{(\mathrm{III})} & h_{22}^{(\mathrm{III})} \end{bmatrix} = \begin{bmatrix} \frac{1}{\bar{y}_{ab}+\bar{y}_{bc}} & \frac{\bar{y}_{bc}}{\bar{y}_{ab}+\bar{y}_{bc}} \\ -\frac{\bar{y}_{bc}}{\bar{y}_{ab}+\bar{y}_{bc}} & \bar{y}_{ac} + \left(\frac{\bar{y}_{bc}\cdot\bar{y}_{ab}}{\bar{y}_{ab}+\bar{y}_{bc}}\right) \end{bmatrix}$$

When $h_{12}^{(\mathrm{I})}$, $h_{12}^{(\mathrm{II})}$, and $h_{12}^{(\mathrm{III})}$ are obtained, L-index of the three cases can be expressed,

$$L_{ac}^{(\mathrm{I})} = |1 - \frac{h_{12}^{(\mathrm{I})}\cdot\bar{v}_{bc}}{\bar{v}_{ac}}| = |1 - \frac{\left(\frac{\bar{y}_{ab}}{\bar{y}_{ab}+\bar{y}_{ac}}\right)\cdot\bar{v}_{bc}}{\bar{v}_{ac}}| \tag{19}$$

$$L_{cb}^{(\mathrm{II})} = |1 - \frac{h_{12}^{(\mathrm{II})}\cdot\bar{v}_{ab}}{\bar{v}_{cb}}| = |1 - \frac{\left(\frac{\bar{y}_{ac}}{\bar{y}_{ac}+\bar{y}_{bc}}\right)\cdot\bar{v}_{ab}}{\bar{v}_{cb}}| \tag{20}$$

$$L_{ba}^{(\mathrm{III})} = |1 - \frac{h_{12}^{(\mathrm{III})}\cdot\bar{v}_{ca}}{\bar{v}_{ba}}| = |1 - \frac{\left(\frac{\bar{y}_{bc}}{\bar{y}_{ab}+\bar{y}_{ab}}\right)\cdot\bar{v}_{ca}}{\bar{v}_{ba}}| \tag{21}$$

On the other hand, by applying (6) to each case, the v-p functions $\overline{\psi}_{ac}^{(\mathrm{I})}$, $\overline{\psi}_{cb}^{(\mathrm{II})}$, and $\overline{\psi}_{ba}^{(\mathrm{III})}$ are given as follows

$$\overline{\psi}_{ac}^{(\mathrm{I})} = \left(\frac{-\bar{y}_{ab}}{\bar{y}_{ab}+\bar{y}_{ac}}\right)\cdot\bar{v}_{bc} \tag{22}$$

$$\overline{\psi}_{cb}^{(\mathrm{II})} = \left(\frac{-\bar{y}_{ac}}{\bar{y}_{ac}+\bar{y}_{bc}}\right)\cdot\bar{v}_{ab} \tag{23}$$

$$\overline{\psi}_{ba}^{(\mathrm{III})} = \left(\frac{-\bar{y}_{bc}}{\bar{y}_{ab}+\bar{y}_{bc}}\right)\cdot\bar{v}_{ca} \tag{24}$$

Hence, L-index and v-p function are related in the following forms.

$$L_{ac}^{(\mathrm{I})} = \left|1 + \frac{\overline{\psi}_{ac}^{(\mathrm{I})}}{\bar{v}_{ac}}\right| \tag{25}$$

$$L_{cb}^{(\mathrm{II})} = \left|1 + \frac{\overline{\psi}_{cb}^{(\mathrm{II})}}{\bar{v}_{cb}}\right| \tag{26}$$

$$L_{ba}^{(\mathrm{III})} = \left|1 + \frac{\overline{\psi}_{ba}^{(\mathrm{III})}}{\bar{v}_{ba}}\right| \tag{27}$$

From the above observation as well as the similarity between L-index defined with the so-called "equivalent-voltage" [29] and its variant having v-p function, we can assume the following relation (see appendix).

$$L_k \propto \left|1 + \frac{\psi_k}{V_k}\right| \tag{28}$$

Let $\gamma$ be a proportional coefficient, and using (12), we have,

$$L_k^2 = \frac{\gamma^2 S_k^2}{Y_{kk}^2 V_k^4} \tag{29}$$

Considering that the power load is constant and hence $\frac{\partial S_k}{\partial \psi_k} = 0$, the derivative of $L_k^2$ with respect to $\psi_k$ can be given as follow.

$$2L_k\frac{\partial L_k}{\partial \psi_k} = -\frac{4\gamma^2 S_k^2}{Y_{kk}^2 V_k^5}\cdot\frac{\partial V_k}{\partial \psi_k} \tag{30}$$

On the other hand, using another arranged form of (12);

$$\frac{S_k^2}{Y_{kk}^2} = V_k^4 + 2\psi_k V_k^3\cos(\Delta_k) + \psi_k^2 V_k^2 \tag{31}$$

$\frac{\partial V_k}{\partial \psi_k}$ is given as the following formula.

$$\frac{\partial V_k}{\partial \psi_k} = -\frac{V_k\,(V_k\cos(\Delta_k) + \psi_k)}{(2V_k + \psi_k)(V_k + \psi_k)} \tag{32}$$

Finally, by substituting (32) into (30), we get,

$$\frac{\partial L_k}{\partial \psi_k} = \frac{2\gamma^2 S_k^2\,(V_k\cos(\Delta_k) + \psi_k)}{L_k Y_{kk}^2 V_k^4 (2V_k + \psi_k)(V_k + \psi_k)} \tag{33}$$

From this formula, it is found that $L_k$ decreases when $\psi_k$ increases if the following condition holds.

$$\cos(\Delta_k) < -\frac{\psi_k}{V_k} \tag{34}$$

### C. POWER LOSS REDUCTION

Power loss by a wire depends on the voltage difference between two ends of the wire, and hence making a lower terminal voltage higher would contribute to reducing the power loss. In addition, a higher voltage can convey the same amount of power with a smaller current, and hence keeping terminal voltages as high as possible would also contribute to power loss reduction. Equation (32) shows that $V_k$ increases when $\psi_k$ increases if the condition (34) again holds.

## IV. PROPOSED METHOD

### A. NORMALIZED VOLTAGE STABILITY INDEX

Several demonstrations in the previous section show the close relation between v-p function and two crucial power system parameters, the L-index for voltage stability measure and power loss. These relationships motivate us to utilize the v-p function as a reliable indicator for identifying RDG locations in both voltage stability and power loss. From the view points of L-index and power loss, the lowest v-p function value over all buses should be maximized. On the other hand, if we consider the relation of v-p function with bus voltage, the gap between the maximum and the minimum of v-p function value over all buses can be an indicator of voltage deviation, which is to be minimized.

Based on these observations, the magnitude of the v-p function normalized by the gap between the maximum and the minimum of v-p function value, which is denoted by $\lambda_k$, is proposed as an indicator of voltage stability and power loss for the $k$th bus.

$$\lambda_k = \frac{\psi_k}{\psi^{\max} - \psi^{\min}} \tag{35}$$

where

$$\psi^{\max} = \max\{\psi_1, \psi_2, \ldots, \psi_N\} \tag{36}$$

$$\psi^{\min} = \min\{\psi_1, \psi_2, \ldots, \psi_N\} \tag{37}$$

For assessing the voltage stability of overall system, the minimum magnitude of the normalized voltage product functions over all buses is utilized and named "Normalized Voltage Stability index ($\Lambda$)," as follows.

$$\Lambda = \min\{\lambda_1, \lambda_2 \cdots, \lambda_N\} \tag{38}$$

### B. LOAD-DISABLING NODAL ANALYSIS

This section presents the proposed method for searching for an optimal location of RDGs. The method is named "Load-Disabling Nodal Analysis (LDNA)," and it consists of two design steps, (1) location determination and (2) size determination.

#### 1) RDG LOCATION DETERMINATION

The primary responsibility of a power distribution system is transferring power from sources to loads with maintaining voltage levels within an acceptable range and keeping power losses as low as possible. Hence the RDG location problem is to find RDG installation locations so that the voltage levels are maintained and power losses are decreased effectively. When a RDG is installed at $k$th bus, it may raise a naive behavioral assumption that the load at $k$th bus may receive a sufficient power from the newly installed RDG, and is hidden from the rest of the power distribution system. It motivates us to observe the system behavior after disconnecting the load from $k$th bus for evaluating the effect of installing a RDG at $k$th bus.

We introduce a vector $(c_1, c_2, \ldots, c_N)$ where $c_k = 0$ means that the load of $k$th bus is disconnected and $c_k = 1$ means otherwise. Note that the number of 0s is no larger than $N_{RDG}$ which is the maximum number of RDGs to be installed. The vector is called the "location vector" hereinafter. Now let $\mathcal{C}$ be the set of all possible location vectors, and the best location(s) of RDG installation ($\mathcal{X}$) is determined by the location vector which maximizes a given objective function $f_o$ over the set $\mathcal{C}$.

$$(c_1^*, c_2^*, \cdots, c_N^*) = \underset{(c_1, c_2, \ldots, c_N) \in \mathcal{C}}{\arg\max} \{f_o((c_1, c_2, \ldots, c_N), lf, \mathrm{RCR})\} \tag{39}$$

and

$$\mathcal{X} = \{k | c_k^* = 0\} \tag{40}$$

(39) should be solved with being subjected to the following constraints.

1. Voltage constraint

   The minimum and the maximum voltage constraints of each bus are expressed as follows.

   $$V^{min} \le V_k \le V^{max}, \quad k \in \mathcal{N} \tag{41}$$

   where $V^{min}$ and $V^{max}$ are taken as 0.95 and 1.05 p.u respectively as given in Refs. [32] and [24].

2. Voltage collapse constraint

   The voltage magnitude at each bus must be greater than its voltage stability limit ($V_k^{SNB}$), since the violation of the constraint results in voltage collapse and system blackout. This constraint is expressed as follows.

   $$V_k^{SNB} < V_k, \quad k \in \mathcal{N} \tag{42}$$

3. Feasibility constraint

   From the voltage equation of (11), $V_k^2$ can be expressed,

   $$V_k^2 = \frac{\psi_k^2 + 2\alpha_k \pm \sqrt{(\psi_k^2 + 2\alpha_k - 2V_k^2)^2}}{2} \tag{43}$$

   Thus, $V_k$ is a feasible solution only if the following equation is satisfied,

   $$\psi_k^2 + 2\alpha_k \pm \sqrt{(\psi_k^2 + 2\alpha_k - 2V_k^2)^2} \ge 0 \tag{44}$$

   $$V_k^2 - \psi_k^2 - 2\alpha_k \le 0, \quad k \in \mathcal{N} \tag{45}$$

#### 2) RDG SIZE DETERMINATION

The total active power produced by RDGs should be no larger than the system's total active power demand because the violation of this constraint results in a reverse power flow in the system [33]. This constraint is expressed as follows.

$$0 \le \sum_{k \in \mathcal{X}} P_k^{RE} \le \sum_{k=1}^{N} P_k \tag{46}$$

After finding the locations $\mathcal{X} = \{G_1, \cdots, G_{|\mathcal{X}|}\}$ of RDGs, the optimal sizes of RDGs are determined so as to minimize the power losses ($P_{loss}^{\mathcal{X}}$), which can be calculated using (3).

$(P_{G_1}^{RE}, \ldots, P_{G_{|\mathcal{X}|}}^{RE})$

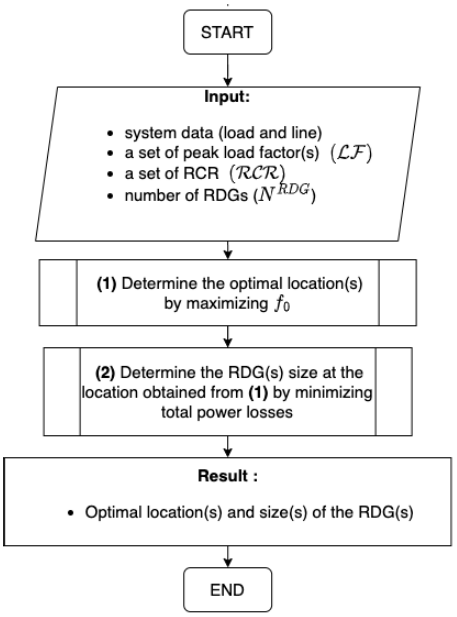


**FIGURE 3.** The overall procedure of Load-disabling Nodal Analysis (LDNA).

$$= \underset{(x_{G_1},\ldots,x_{G_{|\mathcal{X}|}})\in\mathbb{R}^{|\mathcal{X}|}}{\arg\min} \left\{ P^{\mathcal{X}}_{loss}((x_{G_1},\ldots,x_{G_{|\mathcal{X}|}}), \mathrm{RCR}) \right\} \quad (47)$$

(47) should be solved with being subjected to (41), (42), (43) and (46).

In summary, the proposed system design process is described using the flowchart of LDNA which is shown in Fig. 3. First, the information of a power distribution system, i.e., load and line data, a peak load factor, a value of RCR, and the number of RDG(s) to be installed are given. Next, the optimal locations are chosen by maximizing a given objective function which is explained in the next sub-section.

### C. LDNA-RVS: PROPOSED OBJECTIVE FUNCTION

In order to improve the voltage stability after RDG installation, Normalized Voltage Stability index ($\Lambda$) is used as the objective function in LDNA along with RCR$= -0.48$ and lf$= 100\%$.

$$\underset{(c_1,c_2,\cdots,c_N)\in\mathcal{C}}{\arg\max} \{\Lambda((c_1, c_2, \cdots, c_N), lf, RCR)\} \quad (48)$$

The optimization problem given in (48) should be solved with being subjected to(41), (42) and (45).

Locating of RDGs using the Normalized Voltage Stability index as the objective function to be maximized is called LDNA-RVS.

### D. LDNA-QSVS

In [8], another possible objective function, which is named Reactive Power Compensation Support Margin for Voltage Stability Improvement (QSVS), has been proposed. That is, the locating of RDG(s) was formulated as;

$$\underset{(c_1,c_2,\cdots,c_N)\in\mathcal{C}}{\arg\max} \{\mathrm{QSVS}((c_1, c_2, \cdots, c_N), lf, RCR)\} \quad (49)$$

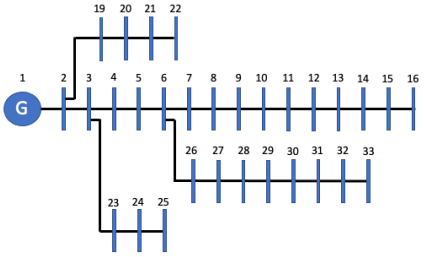


**FIGURE 4.** Single line diagram of the 33-bus test distribution system.

The optimization problem given in (49) should be solved with being subjected to(41), (42) and (45).

Locating of RDGs using the QSVS as the objective function to be maximized is called LDNA-QSVS, and is used as one of the competitors of LDNA-RVS in the following design simulations.

## V. SIMULATIONS AND RESULTS

The proposed method LDNA-RVS is applied to IEEE33- and IEEE 69-bus test distribution systems which are provided by [34] and [35]. For the IEEE33-bus system, Fig. 4 shows the system diagram, which has a total load of 3720 kW and 2300 kVAr at a voltage level of 12.66 kV. Fig. 5 shows the system diagram, which has a total load of 3800 kW and 2690 kVAr at 12.6 kV for the IEEE69-bus system. The information on the maximum levels of power consumption of loads is required when maximum power losses and voltage stability are evaluated. All simulations were carried out using Python programming with a library called PYPSA [36].

We have tested one RDG installation and two RDGs installation for both IEEE33- and IEEE69-bus systems. After the results are obtained, the variations of voltage stability with non-reactive compensation (RCR $= 0$) and maximum reactive compensation (RCR $= -0.48$) are evaluated. Finally, a summary of the simulation results is provided with the two performance indexes, i.e., the loss reduction efficiency (LRE) and voltage stability (VS).

### A. OPTIMAL LOCATIONS AND SIZING

#### 1) ONE RDG INSTALLATION

For one RDG installation, the optimal location and size are obtained via LDNA-RVS. Fig.6 and 7 show the variation of $\Lambda$ for different choices of load disconnecting nodes with a peak load factors 80%, 100%, and 120%. From Fig.6, we can find that disconnecting the 14th bus achieves the maximum $\Lambda$, and hence there is the best location for one RDG installation for IEEE33-bus system. Similarly, Fig.7 indicates that the 61st bus is the best location for one RDG installation in IEEE69-bus system.

By considering the system power losses minimization, the size of RDG installing at the 14th bus is determined at 1151.65kW for IEEE 33-bus system as Fig. 8 shows, and the one at the 61st bus for IEEE 69-bus system is fixed at 1023.81kW as Fig. 9 shows. As a result, in IEEE33-bus

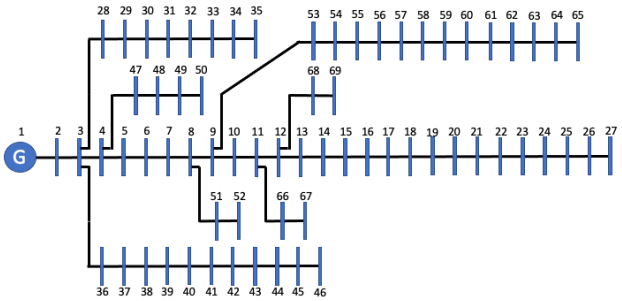


**FIGURE 5.** Single line diagram of the 69-bus test distribution system.

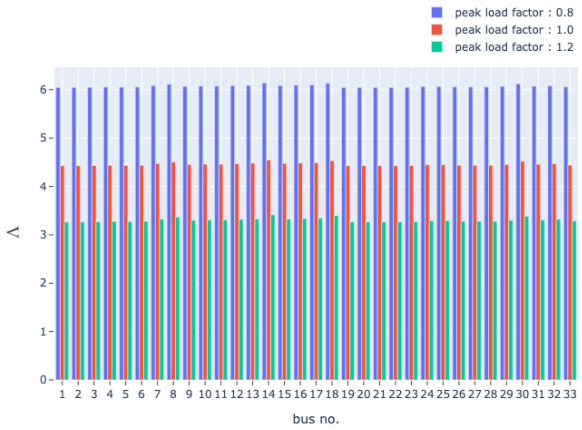


**FIGURE 6.** Variation of Λ at each removal loads and for each peak load factors on IEEE 33-bus test distribution system.

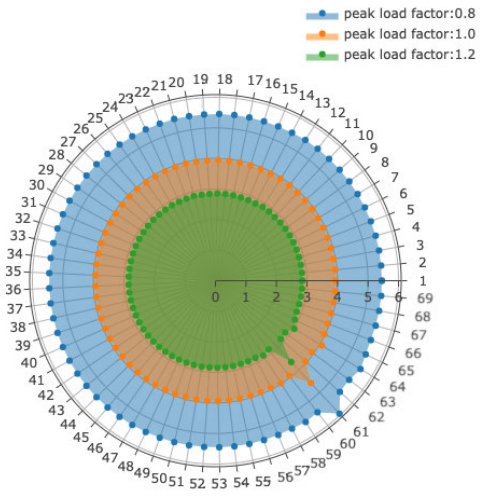


**FIGURE 7.** Variation of Λ at each removal loads and for each peak load factors on IEEE 69-bus test distribution system.

system, the system power loss is decreased from 212.95kW to 178.24kW, which corresponds to power loss reduction efficiency LRE =0.1082. Similarly, for the IEEE 69-bus

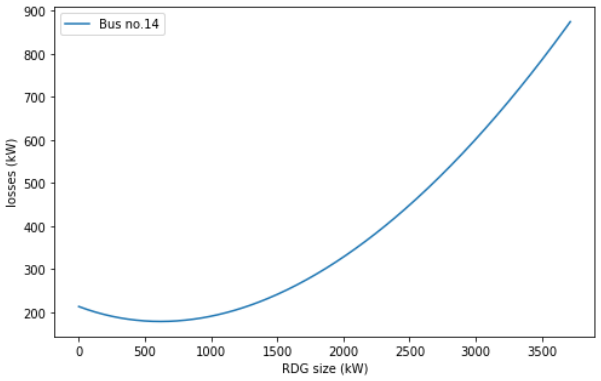


**FIGURE 8.** Variation of power losses with a single RDG for the IEEE 33-bus test distribution system.

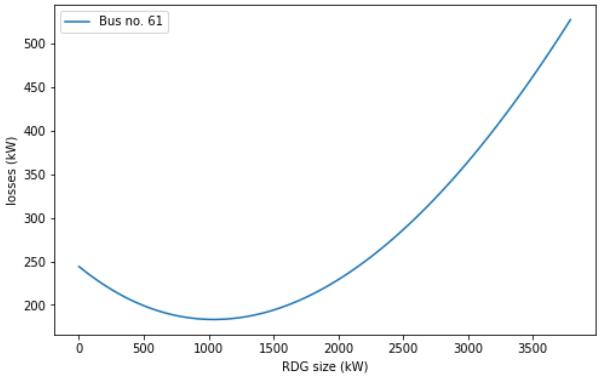


**FIGURE 9.** Variation of power losses with a single RDG for the IEEE 69-bus test distribution system.

system, the system power loss is decreased from 244.16kW to 183.35kW, which corresponds to LRE = 0.1241.

Table 1 and 2 organize the numerical results of the proposed method of LDNA-RVS which are compared with [9], [17], [24], [25], [26], [27], [32], and [8] in terms of LRE and VS.

For the one RDG installation on IEEE33-bus test system, it is found that LDNA-RVS performs the best in LRE and VS when RCR = 0.

For the one RDG installation on IEEE69-bus test system, it is found that LDNA-RVS performs the best in LRE while GA [12] and LDNA-QSVS [8] perform the best in VS when RCR = 0. When we consider the results at RCR = −0.48, it is found that LDNA-RVS performs the best in both LRE and VS.

### 2) TWO RDG LOCATIONS

Next, we have tested two RDGs installation. By considering the maximum increment of Λ after disconnecting loads from candidate node pairs, the 14th and 30th buses are selected as the best locations of two RDGs installation for IEEE33-bus system. Similarly, the 12th and 61st buses are selected for IEEE69-bus system.

**TABLE 1. One RDG integration results for IEEE 33-bus test distribution system.**

| Technique | RDG location (Bus no.) | RDG size (kW) | losses (kW) | RCR = 0 (PF = 1) LRE | RCR = 0 (PF = 1) VS | RCR = -0.48 (PF = -0.9) LRE | RCR = -0.48 (PF = -0.9) VS |
|---|---|---|---|---|---|---|---|
| without | - | - | 212.94 | - | 0.0698 | - | 0.0698 |
| ALGA [24] | 6 | 2580 | 112.68 | 0.0389 | 0.0846 | 0.0059 | 0.0846 |
| BSOA [27] | 8 | 1857.5 | 119.81 | 0.0501 | 0.0771 | 0.0069 | 0.0771 |
| PSO [25] | 6 | 3150 | 116.88 | 0.0305 | 0.0901 | −0.0041 | 0.0901 |
| Analytical [9] | 6 | 2490 | 112.82 | 0.0402 | 0.0838 | 0.0075 | 0.0838 |
| ALOA [32] | 6 | 2450 | 112.96 | 0.0408 | 0.0832 | 0.0082 | 0.0835 |
| WOA [17] | 30 | 1542.67 | 126.92 | 0.0558 | 0.0742 | −0.0006 | 0.0742 |
| MLPSO [26] | 6 | 2420 | 113.09 | 0.0413 | 0.0832 | 0.0087 | 0.0832 |
| LDNA-QSVS [8] | 15 | 1040.2 | 134.71 | 0.0752 | 0.0736 | 0.0152 | 0.0736 |
| **LDNA-RVS (proposed)** | **14** | **1151.65** | **178.24** | **0.1082** | **0.0677** | **0.0922** | **0.0706** |

**TABLE 2. One RDG integration results for IEEE 69-bus test distribution system.**

| Technique | RDG location (Bus no.) | RDG size (kW) | losses (kW) | RCR=0 (PF=1) LRE | RCR=0 (PF=1) VS | RCR=-0.48 (PF=-0.9) LRE | RCR=-0.48 (PF=-0.9) VS |
|---|---|---|---|---|---|---|---|
| without | - | - | 244.16 | - | 0.0960 | - | 0.0960 |
| ABC [10] | 61 | 1900.00 | 88.37 | 0.0819 | 0.0748 | 0.0126 | 0.0923 |
| ALGA [24] | 61 | 1872.00 | 88.32 | 0.0832 | 0.0748 | 0.0140 | 0.0921 |
| Analytical [9] | 61 | 1820.00 | 88.43 | 0.0860 | 0.0749 | 0.0172 | 0.0917 |
| Grid search [11] | 61 | 1807.80 | 88.32 | 0.0831 | 0.0748 | 0.0138 | 0.0921 |
| GA [12] | 61 | 1794.00 | 88.50 | 0.0868 | 0.0748 | 0.0180 | 0.0916 |
| MTLBO [14] | 61 | 1819.69 | 88.39 | 0.0856 | 0.0748 | 0.0167 | 0.0917 |
| BB-BC [15] | 61 | 1872.50 | 88.32 | 0.0832 | 0.0748 | 0.0140 | 0.0921 |
| ALOA [32] | 61 | 1800.00 | 88.47 | 0.0865 | 0.0749 | 0.0177 | 0.0916 |
| LDNA-QSVS [8] | 61 | 1794.00 | 88.50 | 0.0868 | 0.0748 | 0.0180 | 0.0916 |
| **LDNA-RVS (proposed)** | **61** | **1023.81** | **183.35** | **0.1241** | **0.0794** | **0.0594** | **0.0889** |

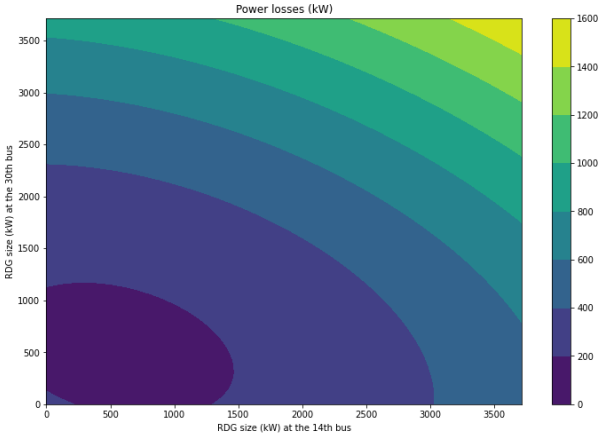


**FIGURE 10. Variation of system losses with two RDGs installation for the IEEE 33-bus test distribution system.**

By considering the system power losses minimization for IEEE 33-bus system, the size at the 14th and 30th buses determined at 520.10kW and 520.10kW (see Fig. 8). As a result, the system power losses are decreased from 212.95kW to 165.91kW, which corresponds to LRE = 0.0959.

For the IEEE 69-bus system, the sizes of RDGs installing at the 12th and 61st buses are respectively determined at 403.60kW and 941.74kW (see Fig. 9). As a result, the system power losses are decreased from 244.16kW to 110.53kW, which corresponds to LRE = 0.0993.

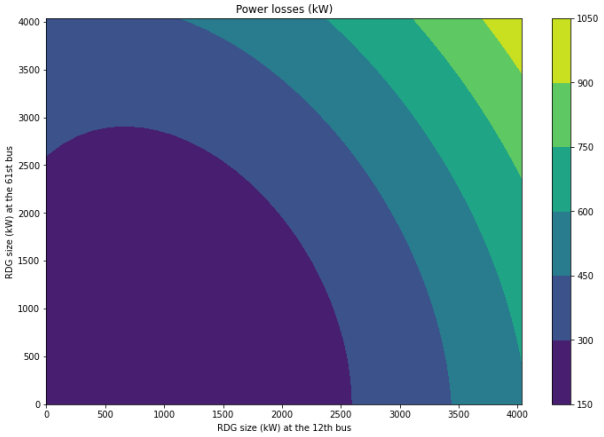


**FIGURE 11. Variation of system losses with two RDGs installation for the IEEE 69-bus test distribution system.**

**TABLE 3. Two RDGs integration results for IEEE 33-bus test distribution system.**

| Technique | RDG location (Bus no.) | RDG size (kW) | losses (kW) | RCR=0 (PF=1.0) LRE | RCR=0 (PF=1.0) VS | RCR=-0.48 (PF=-0.9) LRE | RCR=-0.48 (PF=-0.9) VS |
|---|---|---|---|---|---|---|---|
| Without | - | - | 212.94 | - | 0.0698 | - | 0.0698 |
| ALGA [24] | 13<br>29 | 837.5<br>1212.2 | 87.99 | 0.0610 | 0.0687 | 0.0082 | 0.0787 |
| BSOA [27] | 13<br>31 | 880<br>924 | 90.04 | 0.0681 | 0.0676 | 0.0123 | 0.0764 |
| PSO [25] | 11<br>31 | 2420<br>960 | 171.52 | 0.0123 | 0.0733 | −0.0532 | 0.0913 |
| ALOA [32] | 13<br>30 | 850<br>1191.1 | 87.79 | 0.0613 | 0.0655 | 0.0063 | 0.0770 |
| MLPSO [26] | 13<br>30 | 820<br>1150 | 87.76 | 0.0635 | 0.0654 | 0.0089 | 0.0765 |
| LDNA-QSVS [8] | 15<br>17 | 928.75<br>185.75 | 134.71 | 0.0702 | 0.0683 | 0.0086 | 0.0733 |
| **LDNA-RVS (proposed)** | **14**<br>**30** | **520.10**<br>**520.10** | **165.91** | **0.0959** | **0.0644** | **0.0452** | **0.0703** |

Table 3 shows the comparison of LDNA-RVS with [8], [24], [25], [26], [27], and [32] for IEEE33-bus system in terms of RDG size, power losses, LRE and VS, and it is found that LDNA-RVS performs the best in LRE and VS when RCR = 0.

Similarly, for the two RDGs installation on the IEEE69-bus test system, compared with [14], [23], [24], [32], [37], and [8] in Table 4, LDNA-RVS performs the best result in LRE, while MTLBO [14] performs the best result in VS when RCR = 0.

When we consider the results at RCR = −0.48, it is found that LDNA-RVS performs the best in both LRE and VS.

### *B. LOSS REDUCTION CONSIDERING REACTIVE COMPENSATION*

The minimization of power losses is one major aspect of determining RDGs' optimal placements and can be affected by the uncontrollable reactive compensation of RDGs. The following simulations show the LRE variation of the one and two RDGs installation cases.

#### 1) LOSS REDUCTION OF ONE RDG INTEGRATION

Figs. 12 and 13 show the variation of LRE versus RCR for several different locations and sizes of one RDG

**TABLE 4. Two RDGs integration results for IEEE 69-bus test distribution system.**

| Technique | RDG location (Bus no.) | RDG size (kW) | losses (kW) | RCR=0 (PF=1.0) LRE | RCR=0 (PF=1.0) VS | RCR=-0.48 (PF=-0.9) LRE | RCR=-0.48 (PF=-0.9) VS |
|---|---|---|---|---|---|---|---|
| Without | - | - | 244.15 | - | 0.0960 | - | 0.0960 |
| GA [23] | 61<br>11 | 1777<br>555 | 79.93 | 0.0704 | 0.0741 | 0.0135 | 0.0950 |
| ALGA [24] | 1<br>62 | 6<br>1794 | 89.92 | 0.0857 | 0.0969 | 0.0166 | 0.1082 |
| PSO [38] | 14<br>62 | 700<br>2100 | 101.14 | 0.0841 | 0.0972 | 0.0349 | 0.1073 |
| MTLBO [14] | 17<br>61 | 519.705<br>1732.004 | 76.58 | 0.0744 | 0.0757 | 0.0149 | 0.0956 |
| ALOA [32] | 17<br>61 | 538.777<br>1700 | 76.74 | 0.0748 | 0.0758 | 0.0158 | 0.0956 |
| LDNA-QSVS [8] | 60<br>61 | 201.8<br>1614.42 | 76.73 | 0.0859 | 0.0759 | 0.0178 | 0.0925 |
| **LDNA-RVS (proposed)** | **12**<br>**61** | **403.60**<br>**941.74** | **110.53** | **0.0993** | **0.0783** | **0.0483** | **0.0899** |

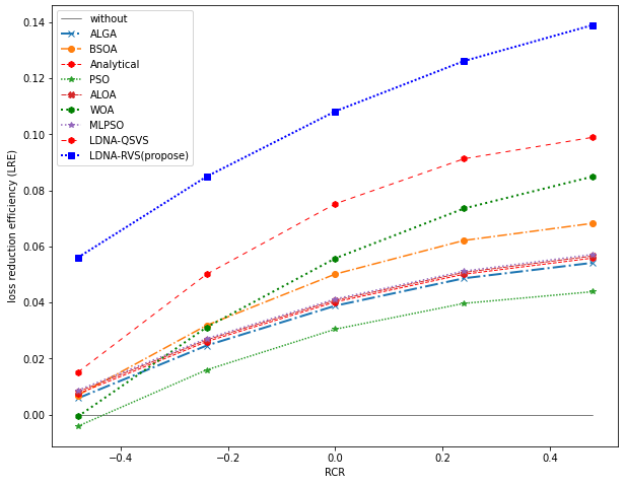


**FIGURE 12. Variation of LRE of the IEEE 33-bus system with reactive compensations of 1 RDG.**

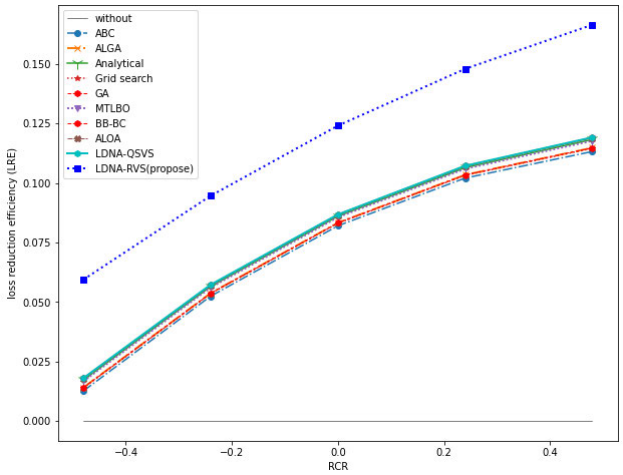


**FIGURE 13. Variation of LRE of the IEEE 69-bus system with reactive compensations of 1 RDG.**

installation in IEEE33-bus system and IEEE69-bus system, respectively. Based on these results, the variation

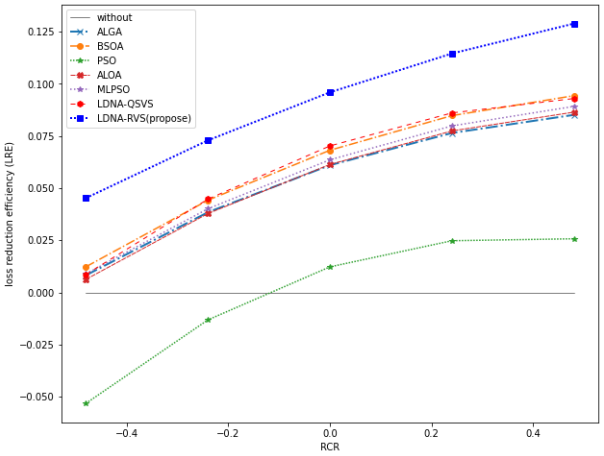


**FIGURE 14. Variation of LRE of the IEEE 33-bus system with reactive compensations of 2 RDG.**

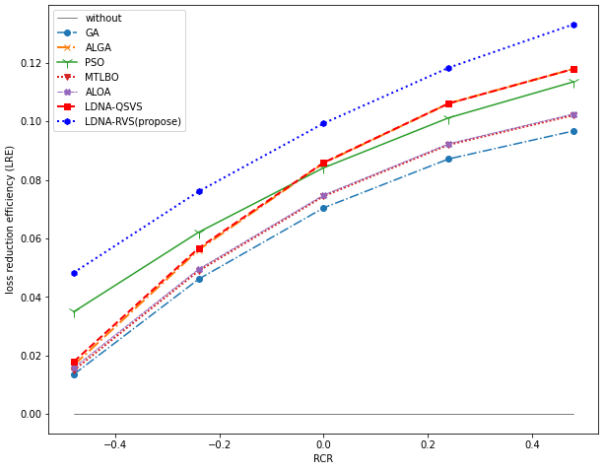


**FIGURE 15. Variation of LRE of the IEEE 69-bus system with reactive compensations of 2 RDG.**

of function LRE appears to be decreased directly proportional to the capacity of reactive compensation of RDGs. Another point is that, even if the location of RDG installation is identical, different size of RDG may yield different LRE.

### 2) LOSS REDUCTION OF 2 RDGs INTEGRATION

Figs. 14 and 15 show the variation of LRE for different locations and sizes of RDGs installation. Here we can observe the similar characteristics on LRE with those in the case of one RDG installation.

While RDGs compensate for the reactive power to maintain the voltage level at the operating point, their LRE is reduced and the power losses may increase, as we can see such examples PSO [25] and WOA [17] in Figs. 12 and 14. Therefore, to avoid increasing losses against the fluctuation of RDGs, LRE of them needs to be considered within the target range of reactive compensation.

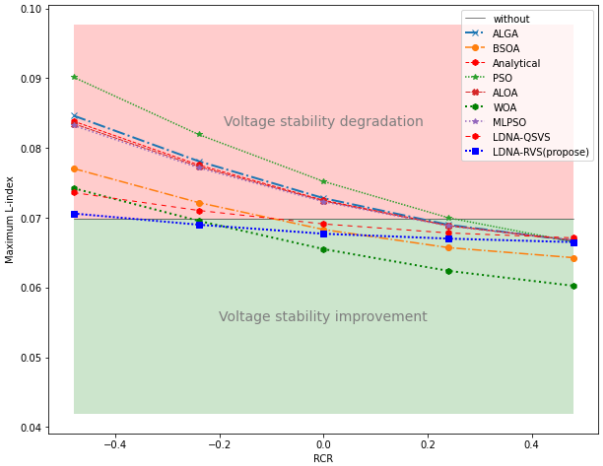


**FIGURE 16.** Variation of voltage stability of the IEEE 33-bus system with reactive compensations of 1 RDG using maximum L-index.

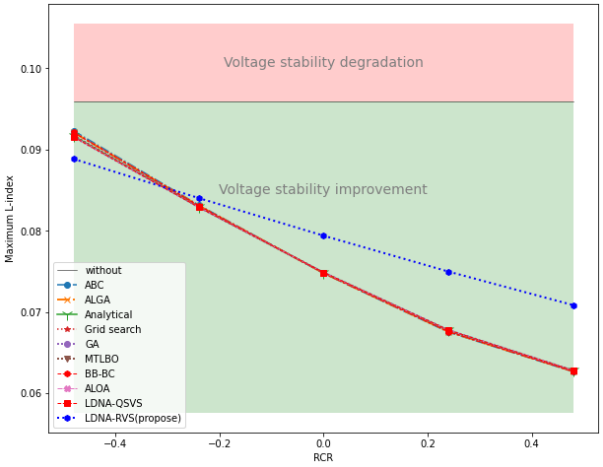


**FIGURE 17.** Variation of voltage stability of the IEEE 69-bus system with reactive compensations of 1 RDG using maximum L-index.

### C. VOLTAGE STABILITY CONSIDERING REACTIVE COMPENSATION

Figs.16 and 17 show the variations of voltage stability measured by L-index versus RCR for different solutions of RDG installation. Similar to LRE characteristics, L-index is monotonic with respect to RCR, and the worst voltage stability happens at RCR $= -0.48$, the smallest end of RCR under consideration. Most solutions of one RDG installation stay in the region of voltage stability improvement for RCR larger than 0 in IEEE33-bus system and for all range of RCR in IEEE69-bus system. We also found that the solution by our proposed LDNA-RVS performs the best in the voltage stability at RCR $= -0.48$, and it goes across the border between stability degradation and improvement at the smallest RCR compared with other solutions.

Figs. 18 and 19 show voltage stability characteristics versus RCR achieved by solutions of two RDGs installation, and we can find the similar tendency with one RDG installation case. Here we also observe the superiority of the solution by our LDNA-RVS in voltage stability.

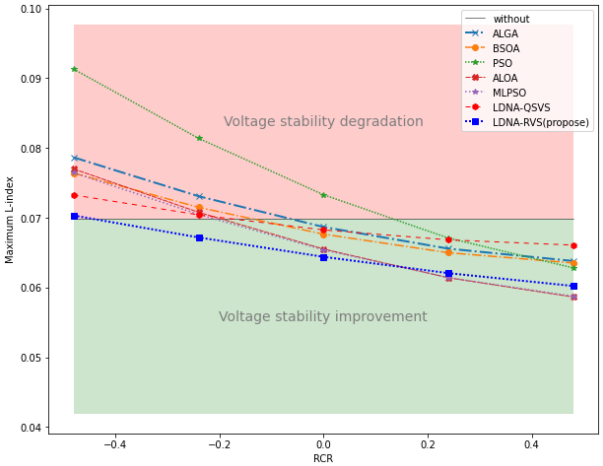


**FIGURE 18.** Variation of voltage stability of the IEEE 33-bus system with reactive compensations of 2 RDGs using maximum L-index.

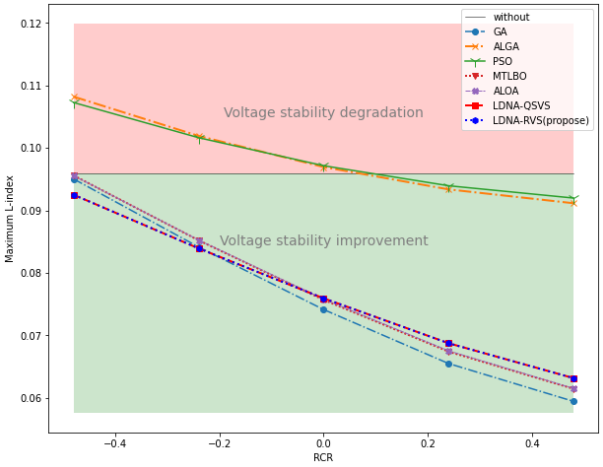


**FIGURE 19.** Variation of voltage stability of the IEEE 69-bus system with reactive compensations of 2 RDGs using maximum L-index.

**TABLE 5.** List of best solutions with respect to LRE and VS at RCR = 0 and RCR = −0.48.

| Case | LRE | | VS | | Increase loss | |
|---|---|---|---|---|---|---|
| | RCR = 0 | RCR=-0.48 | RCR = 0 | RCR=-0.48 | RCR = 0 | RCR=-0.48 |
| IEEE33 (1 RDG) | **LDNA-RVS (proposed)** | **LDNA-RVS (proposed)** | **LDNA-RVS (proposed)** | **LDNA-RVS (proposed)** | - | PSO [25], WOA [37] |
| IEEE69 (1 RDG) | **LDNA-RVS (proposed)** | **LDNA-RVS (proposed)** | GA[12], LDNA-QSVS [8] | **LDNA-RVS (proposed)** | - | PSO [25] |
| IEEE33 (2 RDGs) | **LDNA-RVS (proposed)** | **LDNA-RVS (proposed)** | **LDNA-RVS (proposed)** | **LDNA-RVS (proposed)** | - | - |
| IEEE69 (2 RDGs) | **LDNA-RVS (proposed)** | **LDNA-RVS (proposed)** | MTLBO[14] | **LDNA-RVS (proposed)** | - | - |

### D. SUMMARY RESULTS

Table 5 shows the list of best solutions with respect to LRE and VS at RCR $= 0$ and RCR $= -0.48$. Our proposed LDNA-RVS takes the first place at 8 categories out of 8 categories in LRE, and at 6 categories out of 8 categories in VS. On the other hand, LDNA-QSVS, GA [12] and MTLBO [14] take the first place at an only one category in VS. Finally, our proposed LDNA-RVS performs the best in LRE

and supports the robustness of voltage stability overall in the reactive compensation.

## VI. CONCLUSION

After examining Tables 1, 3, 2, and 4, it becomes evident that increased reactive compensation in Reactive Distribution Generators (RDGs) leads to a decrease in voltage stability variation, which is accompanied by a decline in loss reduction efficiency. Therefore, voltage stability improvement plays an important role not only in ensuring effective power delivery and mitigating the risk of voltage collapse but also in reducing losses within the system. Nevertheless, the power loss minimization does not always contribute to voltage stability improvement. Throughout the discussions and simulations in this paper, our proposed voltage stability index($\Lambda$) is confirmed to work well for finding the locations of RDGs installation in both voltage stability improvement and power loss reduction efficiency. While the placement of RDGs has been mainly addressed in this paper, the proposed LDNA is applicable to the placement of DGs and that of the mixture of DGs and RDGs if their reactive power compensation ratios are explicitly specified.

### FUTURE RESEARCH DIRECTIONS

Several issues need to be addressed in future work to further improve the applicability and performance of the proposed method.

Firstly, it is crucial to reduce the time complexity of the Load Distribution Network Algorithm (LDNA), particularly for large-scale power systems. This is because the time complexity is dependent on the size of the power system and exponentially dependent on the number of RDGs to be installed. One practical solution to this issue could be to the elimination of computations, such as by skipping unpromising candidate locations for RDGs.

Secondly, considering the crucial role that energy storage devices play in absorbing the fluctuations of RDGs, it is essential to extend the proposed method to power systems that incorporate these storage devices. This will help overcome the serious issues associated with uncontrollable reactive compensation and environment-dependent changes. Additionally, exploring the application or extension of the proposed method to the location and sizing of energy storage devices could be a valuable area for future research.

## APPENDIX

### A. EXPLANATION OF EQUATION (28)

L-index has been defined in the following way in [29]. For a given system, at first, nodes are separated into the set $\alpha_G$ of generator nodes and the set $\alpha_L$ of consumer nodes, and a system equation in terms of a hybrid matrix as follows.

$$\begin{pmatrix} \boldsymbol{V}^L \\ \boldsymbol{I}^G \end{pmatrix} = \begin{pmatrix} \boldsymbol{Z}^{LL} & \boldsymbol{F}^{LG} \\ \boldsymbol{K}^{GL} & \boldsymbol{Y}^{GG} \end{pmatrix} \begin{pmatrix} \boldsymbol{I}^L \\ \boldsymbol{V}^G \end{pmatrix} \tag{50}$$

$\boldsymbol{V}^L$ and $\boldsymbol{I}^L$ are vectors of voltages and currents, respectively, at consumer nodes, $\boldsymbol{V}^G$ and $\boldsymbol{I}^G$ are vectors of voltages and currents, respectively, at generator nodes, and $\boldsymbol{Z}^{LL}$, $\boldsymbol{F}^{LG}$, $\boldsymbol{K}^{GL}$ and $\boldsymbol{Y}^{GG}$ are submatrices of the hybrid matrix. Then, for any consumer node $k$, $k \in \alpha_L$, its voltage $\overline{V}_k$ is represented as follows.

$$\overline{V}_k = \sum_{n\in\alpha_L} \overline{Z}_{kn} \cdot \overline{I}_n + \sum_{n\in\alpha_G} \overline{F}_{kn} \cdot \overline{V}_n \tag{51}$$

Now, by multiplying $\overline{V}_k^*$ to both side of the equaiton, we get,

$$\begin{aligned} V_k^2 &= \left(\sum_{n\in\alpha_L} \overline{Z}_{kn} \cdot \overline{I}_n\right)\overline{V}_k^* + \left(\sum_{n\in\alpha_G} \overline{F}_{kn} \cdot \overline{V}_n\right)\overline{V}_k^* \\ &= \overline{Z}_{kk}\left(\sum_{\substack{n\in\alpha_L \\ n\neq k}} \frac{\overline{Z}_{kn}}{\overline{Z}_{kk}} \cdot \frac{\overline{S}_n^*}{\overline{V}_n^*}\right)\overline{V}_k^* + \overline{Z}_{kk} \cdot \overline{I}_k \cdot \overline{V}_k^* \\ &\quad -\left(-\sum_{n\in\alpha_G} \overline{F}_{kn} \cdot \overline{V}_n\right)\overline{V}_k^* \\ &= \frac{\left(\overline{S}_k^{corr} + \overline{S}_k\right)^*}{\overline{Y}_{kk}} - \overline{V}_{0k} \cdot \overline{V}_k^* \end{aligned} \tag{52}$$

where

$$\overline{S}_k^{corr} = \left(\sum_{\substack{n\in\alpha_L \\ n\neq k}} \frac{\overline{Z}_{kn}^*}{\overline{Z}_{kk}^*} \cdot \frac{\overline{S}_n}{\overline{V}_n}\right)\overline{V}_k \tag{53}$$

$$\overline{Y}_{kk} = \frac{1}{\overline{Z}_{kk}} \tag{54}$$

$$\overline{V}_{0k} = -\sum_{n\in\alpha_G} \overline{F}_{kn} \cdot \overline{V}_n \tag{55}$$

From (52), we have,

$$1 + \frac{\overline{V}_{0k}}{\overline{V}_k} = \frac{\left(\overline{S}_k^{corr} + \overline{S}_k\right)^*}{\overline{Y}_{kk} \cdot V_k^2} \tag{56}$$

Finally, L-index has been defined as follows.

$$L_k = \left|1 - \frac{\sum_{n\in\alpha_G} \overline{F}_{kn} \cdot \overline{V}_n}{\overline{V}_k}\right| \tag{57}$$

$$= \left|1 + \frac{\overline{V}_{0k}}{\overline{V}_k}\right| \tag{58}$$

$$= \left|\frac{\left(\overline{S}_k^{corr} + \overline{S}_k\right)^*}{\overline{Y}_{kk} \cdot V_k^2}\right| \tag{59}$$

Recall that a power system is a linear time invariant circuit, and now we limit our discussion on a system excited by a single generator whose voltage is $\overline{V}_G$. Due to the linearity of the circuit, every current $\overline{I}_n$ can be represented as the product of $\overline{T}_n$, the transfer conductance from the generator to the $n$th bus current, and $\overline{V}_G$. Accordingly, we have the following.

$$\overline{I}_n = \overline{T}_n \cdot \overline{V}_G = \frac{\overline{T}_n}{\overline{T}_k} \cdot \overline{T}_k \cdot \overline{V}_G = \frac{\overline{T}_n}{\overline{T}_k} \cdot \overline{I}_k \tag{60}$$

Consequently, $\overline{S}_k^{corr}$ can be related to $\overline{S}_k$ in the following form.

$$\begin{aligned}
\overline{S}_k^{corr} &= \left( \sum_{\substack{n\in\alpha_L \\ n\neq k}} \frac{\overline{Z}_{kn}^*}{\overline{Z}_{kk}^*} \cdot \frac{\overline{S}_n}{\overline{V}_n} \right) \overline{V}_k \\
&= \left( \sum_{\substack{n\in\alpha_L \\ n\neq k}} \frac{\overline{Z}_{kn}^*}{\overline{Z}_{kk}^*} \cdot \overline{I}_n^* \right) \overline{V}_k \\
&= \left( \sum_{\substack{n\in\alpha_L \\ n\neq k}} \frac{\overline{Z}_{kn}^*}{\overline{Z}_{kk}^*} \cdot \frac{\overline{T}_n^*}{\overline{T}_k^*} \cdot \overline{I}_k^* \right) \overline{V}_k \\
&= \left( \sum_{\substack{n\in\alpha_L \\ n\neq k}} \frac{\overline{Z}_{kn}^*}{\overline{Z}_{kk}^*} \cdot \frac{\overline{T}_n^*}{\overline{T}_k^*} \right) \overline{S}_k \qquad (61) \\
1 + \frac{\overline{V}_{0k}}{\overline{V}_k} &= \frac{\left( \overline{S}_k^{corr} + \overline{S}_k \right)^*}{\overline{Y}_{kk} \cdot V_k^2} \\
&= \frac{(W_{kn}+1)^* \cdot \overline{S}_k^*}{\overline{Y}_{kk} \cdot V_k^2} \qquad (62)
\end{aligned}$$

where

$$W_{kn} = \sum_{\substack{n\in\alpha_L \\ n\neq k}} \frac{\overline{Z}_{kn}^*}{\overline{Z}_{kk}^*} \cdot \frac{\overline{T}_n^*}{\overline{T}_k^*} \qquad (63)$$

Finally,

$$\begin{aligned}
L_k &= \left| \frac{\left( \overline{S}_k^{corr} + \overline{S}_k \right)^*}{\overline{Y}_{kk} \cdot V_k^2} \right| \\
&= |W_{kn}+1| \cdot \left| \frac{\overline{S}_k^*}{\overline{Y}_{kk} \cdot V_k^2} \right| \\
&= |W_{kn}+1| \cdot \left| 1 + \frac{\overline{\psi}_k}{\overline{V}_k} \right| \qquad (64)
\end{aligned}$$

## REFERENCES


[1] J. Floyd and K. Zubevich, "Linking foresight and sustainability: An integral approach," *Futures*, vol. 42, no. 1, pp. 59–68, Feb. 2010. [Online]. Available: https://www.sciencedirect.com/science/article/pii/S0016328709001414

[2] R. Luna-Rubio, M. Trejo-Perea, D. Vargas-Vázquez, and G. J. Ríos-Moreno, "Optimal sizing of renewable hybrids energy systems: A review of methodologies," *Sol. Energy*, vol. 86, no. 4, pp. 1077–1088, Apr. 2012.

[3] F.-L. Xu, S.-S. Zhao, R. W. Dawson, J.-Y. Hao, Y. Zhang, and S. Tao, "A triangle model for evaluating the sustainability status and trends of economic development," *Ecological Model.*, vol. 195, nos. 3–4, pp. 327–337, Jun. 2006.

[4] G. Pepermans, J. Driesen, D. Haeseldonckx, R. Belmans, and W. D'haeseleer, "Distributed generation: Definition, benefits and issues," *Energy Policy*, vol. 33, no. 6, pp. 787–798, Apr. 2005.

[5] T. Ackermann, G. Andersson, and L. Söder, "Distributed generation: A definition," *Electr. Power Syst. Res.*, vol. 57, no. 3, pp. 195–204, Apr. 2001.

[6] G. J. Dalton, D. A. Lockington, and T. E. Baldock, "Case study feasibility analysis of renewable energy supply options for small to medium-sized tourist accommodations," *Renew. Energy*, vol. 34, no. 4, pp. 1134–1144, Apr. 2009, doi: 10.1016/j.renene.2008.06.018.

[7] P. Yilmaz, M. Hakan Hocaoglu, and A. E. S. Konukman, "A pre-feasibility case study on integrated resource planning including renewables," *Energy Policy*, vol. 36, no. 3, pp. 1223–1232, Mar. 2008.

[8] A. Kwangkaew, S. Javaid, C. Charoenlarpnopparut, and M. Kaneko, "Optimal location and sizing of renewable distributed generators for improving voltage stability and security considering reactive power compensation," *Energies*, vol. 15, no. 6, p. 2126, Mar. 2022. [Online]. Available: https://www.mdpi.com/1996-1073/15/6/2126

[9] N. Acharya, P. Mahat, and N. Mithulananthan, "An analytical approach for DG allocation in primary distribution network," *Int. J. Electr. Power Energy Syst.*, vol. 28, no. 10, pp. 669–678, Dec. 2006.

[10] L. D. Arya, A. Koshti, and S. C. Choube, "Distributed generation planning using differential evolution accounting voltage stability consideration," *Int. J. Electr. Power Energy Syst.*, vol. 42, no. 1, pp. 196–207, Nov. 2012.

[11] T. Gözel and M. H. Hocaoglu, "An analytical method for the sizing and siting of distributed generators in radial systems," *Electr. Power Syst. Res.*, vol. 79, no. 6, pp. 912–918, Jun. 2009.

[12] I. Pisica, C. Bulac, and M. Eremia, "Optimal distributed generation location and sizing using genetic algorithms," in *Proc. 15th Int. Conf. Intell. Syst. Appl. Power Syst.*, Curitiba, Brazil, 2009, pp. 1–6, doi: 10.1109/ISAP.2009.5352936.

[13] D. K. Khatod, V. Pant, and J. Sharma, "Evolutionary programming based optimal placement of renewable distributed generators," *IEEE Trans. Power Syst.*, vol. 28, no. 2, pp. 683–695, May 2013.

[14] J. A. M. García and A. J. G. Mena, "Optimal distributed generation location and size using a modified teaching–learning based optimization algorithm," *Int. J. Electr. Power Energy Syst.*, vol. 50, pp. 65–75, Sep. 2013.

[15] A. Y. Abdelaziz, Y. G. Hegazy, W. El-Khattam, and M. M. Othman, "A multi-objective optimization for sizing and placement of voltage-controlled distributed generation using supervised big bang–big crunch method," *Electr. Power Compon. Syst.*, vol. 43, no. 1, pp. 105–117, Jan. 2015.

[16] E. S. Ali, S. M. A. Elazim, and A. Y. Abdelaziz, "Optimal allocation and sizing of renewable distributed generation using ant lion optimization algorithm," *Electr. Eng.*, vol. 100, no. 1, pp. 99–109, Mar. 2018.

[17] V. C. V. Reddy, "Optimal renewable resources placement in distribution networks by combined power loss index and whale optimization algorithms," *J. Electr. Syst. Inf. Technol.*, vol. 5, no. 2, pp. 175–191, Sep. 2018.

[18] D. Q. Hung, N. Mithulananthan, and K. Y. Lee, "Optimal placement of dispatchable and nondispatchable renewable DG units in distribution networks for minimizing energy loss," *Int. J. Electr. Power Energy Syst.*, vol. 55, pp. 179–186, Feb. 2014, doi: 10.1016/j.ijepes.2013.09.007.

[19] H. HassanzadehFard and A. Jalilian, "Optimal sizing and location of renewable energy based DG units in distribution systems considering load growth," *Int. J. Electr. Power Energy Syst.*, vol. 101, pp. 356–370, Oct. 2018, doi: 10.1016/j.ijepes.2018.03.038.

[20] R. W. Chang, N. Mithulananthan, and T. K. Saha, "Novel mixed-integer method to optimize distributed generation mix in primary distribution systems," in *Proc. AUPEC*, 2011, pp. 1–6.

[21] A. F. A. Kadir, A. Mohamed, H. Shareef, A. A. Ibrahim, T. Khatib, and W. Elmenreich, "An improved gravitational search algorithm for optimal placement and sizing of renewable distributed generation units in a distribution system for power quality enhancement," *J. Renew. Sustain. Energy*, vol. 6, no. 3, pp. 1–18, 2014.

[22] M. Milovanović, D. Tasić, J. Radosavljević, and B. Perović, "Optimal placement and sizing of inverter-based distributed generation units and shunt capacitors in distorted distribution systems using a hybrid phasor particle swarm optimization and gravitational search algorithm," *Electr. Power Compon. Syst.*, vol. 48, nos. 6–7, pp. 543–557, Apr. 2020, doi: 10.1080/15325008.2020.1797934.

[23] T. N. Shukla, S. P. Singh, V. Srinivasarao, and K. B. Naik, "Optimal sizing of distributed generation placed on radial distribution systems," *Electr. Power Compon. Syst.*, vol. 38, no. 3, pp. 260–274, Jan. 2010.

[24] A. A. Hassan, F. H. Fahmy, A. E.-S.-A. Nafeh, and M. A. Abu-elmagd, "Genetic single objective optimisation for sizing and allocation of renewable DG systems," *Int. J. Sustain. Energy*, vol. 36, no. 6, pp. 545–562, Jul. 2017.

[25] S. Kansal, V. Kumar, and B. Tyagi, "Optimal placement of different type of DG sources in distribution networks," *Int. J. Electr. Power Energy Syst.*, vol. 53, pp. 752–760, Dec. 2013.

[26] E. Karunarathne, J. Pasupuleti, J. Ekanayake, and D. Almeida, "Optimal placement and sizing of DGs in distribution networks using MLPSO algorithm," *Energies*, vol. 13, no. 23, p. 6185, Nov. 2020.
[27] A. El-Fergany, "Optimal allocation of multi-type distributed generators using backtracking search optimization algorithm," *Int. J. Electr. Power Energy Syst.*, vol. 64, pp. 1197–1205, Jan. 2015.
[28] T. V. Cutsem and C. Vournas, *Voltage Stability of Electric Power Systems*. Boston, MA, USA: Springer, 1998.
[29] P. Kessel and H. Glavitsch, "Estimating the voltage stability of a power system," *IEEE Trans. Power Del.*, vol. PD-1, no. 3, pp. 346–354, Jul. 1986.
[30] D. Q. Hung and N. Mithulananthan, "Multiple distributed generator placement in primary distribution networks for loss reduction," *IEEE Trans. Ind. Electron.*, vol. 60, no. 4, pp. 1700–1708, Apr. 2013.
[31] N. Hosseinzadeh, A. Aziz, A. Mahmud, A. Gargoom, and M. Rabbani, "Voltage stability of power systems with renewable-energy inverter-based generators: A review," *Electronics*, vol. 10, no. 2, pp. 1–27, 2021, doi: 10.3390/electronics10020115.
[32] E. S. Ali, S. M. A. Elazim, and A. Y. Abdelaziz, "Ant lion optimization algorithm for optimal location and sizing of renewable distributed generations," *Renew. Energy*, vol. 101, pp. 1311–1324, Feb. 2017.
[33] I. B. Majeed and N. I. Nwulu, "Impact of reverse power flow on distributed transformers in a solar-photovoltaic-integrated low-voltage network," *Energies*, vol. 15, no. 23, p. 9238, Dec. 2022. [Online]. Available: https://www.mdpi.com/1996-1073/15/23/9238
[34] D. Das, D. P. Kothari, and A. Kalam, "Simple and efficient method for load flow solution of radial distribution networks," *Int. J. Electr. Power Energy Syst.*, vol. 17, no. 5, pp. 335–346, Oct. 1995. [Online]. Available: https://www.sciencedirect.com/science/article/pii/0142061595000500
[35] M. E. Baran and F. F. Wu, "Optimal capacitor placement on radial distribution systems," *IEEE Trans. Power Del.*, vol. 4, no. 1, pp. 725–734, Jan. 1989.
[36] T. Brown, J. Hörsch, and D. Schlachtberger, "PyPSA: Python for power system analysis," *J. Open Res. Softw.*, vol. 6, no. 1, p. 4, Jan. 2018, doi: 10.5334/jors.188.
[37] W. S. Tan, M. Y. Hassan, M. S. Majid, and H. A. Rahman, "Allocation and sizing of DG using cuckoo search algorithm," in *Proc. IEEE Int. Conf. Power Energy (PECon)*, Dec. 2012, pp. 133–138.

**AKANIT KWANGKAEW** received the B.S. degree in electrical engineering from Kasetsart University, Thailand, in 2012, and the M.Eng. degree in information and communication technology for embedded systems from the Sirindhorn International Institute of Technology, Thammasat University, Thailand, in 2017. He is currently pursuing the dual Ph.D. degrees in information science and engineering and technology with the Japan Advanced Institute of Science and Technology, Japan, and the Sirindhorn International Institute of Technology, Thammasat University. His research interests include smart grid systems, renewable energy resources, voltage stability, energy informatics, and its application in power systems.

**SIRIYA SKOLTHANARAT** received the B.S. degree in electrical engineering from the King Mongkut's Institute of Technology Ladkrabang, Thailand, in 1999, the M.S. degree in electric power engineering from Rensselaer Polytechnic Institute, in 2003, and the Ph.D. degree from Virginia Polytechnic Institute and State University (Virginia Tech). Currently, she is a Researcher with the National Electronics and Computer Technology Center (NECTEC), National Science and Technology Development Agency, Thailand. Her research interests include renewable energy resources, energy management systems, and power quality in power systems.

**CHALIE CHAROENLARPNOPPARUT** received the B.Eng. degree (Hons.) in electrical engineering from Chulalongkorn University, Thailand, in 1993, and the M.S. and Ph.D. degrees in electrical engineering from Pennsylvania State University, PA, USA, in 1995 and 2000, respectively. From 1999 to 2001, he was a Research Assistant, a Lecturer, and an Assistant Professor with The Pennsylvania State University. Currently, he is an Associate Professor with the School of Information Computer and Communication Technology (ICT), SIIT, Thammasat University. His research interests include multidimensional signal processing, image processing, signal processing for communication, and smart grid systems. He received the Gold Medal during his bachelor's degree.

**MINEO KANEKO** (Member, IEEE) received the B.E., M.E., and Dr.E. degrees in electrical and electronic engineering from the Tokyo Institute of Technology, Tokyo, Japan, in 1981, 1983, and 1986, respectively. From 1986 to 1996, he was with the Department of Electrical and Electronic Engineering, Tokyo Institute of Technology, as a Research Associate, a Lecturer, and an Associate Professor. Currently, he is a Professor with the School of Information Science, Japan Advanced Institute of Science and Technology, Ishikawa, Japan. His research interests include circuit theory and computer-aided-design for VLSIs, fault tolerant VLSI parallel computing toward dependable ULSI/WSI, and analog/digital signal processing with an emphasis on VLSI implementation.